Journal of Glaciology, Vol. 8, No. 52, 1969

GEODETIC RESULTS OF THE ROSS ICE SHELF SURVEY EXPEDITIONS, 1962–63 AND 1965–66

By EGON DORRER, WALTHER HOFMANN *and* WILFRIED SEUFERT

(Lehrstuhl für Photogrammetrie und Kartographie, Technische Universität Braunschweig, 33 Braunschweig, West Germany)

ABSTRACT. By means of modern geodetic observation techniques the ice movement along an east–west and a north–south profile across the Ross Ice Shelf, Antarctica, was measured during the two Antarctic summers, 1962–63 and 1965–66. 103 markers were placed on the 910 km long traverse. Distances were measured by tellurometer, and traverse angles by a precision theodolite between all consecutive markers, normally 8 to 9 km apart. For this type of observation method, six men distributed into three groups of two men each were necessary.

The main part of the paper deals with data processing and with the computation of the ice movement. As the ice moves, the geometrical configuration of the traverse changes during the epoch of observation. For this "reduction to epoch" problem two methods are described in detail: (1) time reduction of observations, and (2) time reduction of positions. Between the two field journeys, only linear ice movement can be assumed. It is possible, however, to determine acceleration and curvature of the ice flow at all traverse points where the traverse angles differ considerably from 180°.

The result of all computations is the field of velocity vectors along the traverse. Obvious characteristics are the rapid increase of velocity between the McMurdo Ice Shelf and Ross Ice Shelf, the uniform and nearly parallel movement in the middle of the ice shelf (maximum velocity 935 m year^{-1}), the decrease of velocity along the north–south profile, and the systematic increase of divergence of the flow lines towards the ice margins. Careful study of the velocity vector field shows some deviations from an entirely uniform distribution.

RÉSUMÉ. *Résultats géodésiques des Ross Ice Shelf Survey expéditions, 1962–63 et 1965–66.* Au moyen de techniques d'observations géodésiques modernes, le mouvement de la glace le long de profils est–ouest et nord–sud sur le Ross Ice Shelf, Antarctique, a été mesuré durant les deux étés antarctiques 1962–63 et 1965–66. Au total, 103 balises ont été placées sur une distance de 910 km. Les distances étaient mesurées à l'aide de telluromètres, et les angles à l'aide d'un théodolite de précision à chaque balise, normalement distantes de 8 à 9 km. Pour ce type de méthode d'observation, 6 personnes réparties en trois groupes de deux étaient nécessaires.

Le chapitre principal porte sur l'exploitation des données et la détermination du mouvement de la glace. Comme la glace s'écoule, la configuration géométrique de la polygonale change pendant la période d'observation. Pour ce problème de réduction dans le temps, deux méthodes sont décrites en détail: (1) réduction du temps des observations et (2) réduction du temps des positions. Entre les deux campagnes, un mouvement linéaire de la glace peut seul être admis. Il est cependant possible de déterminer l'accélération et la courbure de l'écoulement de la glace en chaque point de la polygonale où les angles diffèrent beaucoup de 180°.

Le résultat obtenu est le champ des vecteurs vitesse le long de la polygonale. Les caractéristiques marquantes sont l'augmentation de vitesse entre McMurdo et le Ross Ice Shelf, le mouvement uniforme et quasi parallèle au milieu de l'ice shelf (maximum 935 m an^{-1}), la diminution de la vitesse le long du profil nord–sud, et la divergence systématique des lignes d'écoulement vers les bords de la glace. L'étude soignée du champ des vecteurs de vitesse montre quelques déviations d'une distribution entièrement uniforme.

ZUSAMMENFASSUNG. *Geodätische Ergebnisse der Ross Ice Shelf Survey Expeditionen, 1962–63 und 1965–66.* Mit Hilfe moderner geodätischer Beobachtungsmethoden wurde während der zwei Südsommer 1962–63 und 1965–66 die Eisbewegung längs eines Ostwest- und eines Nordsüd-Profils auf dem Ross Ice Shelf, Antarktis, bestimmt. Insgesamt wurden auf der 910 km langen Strecke 103 Geschwindigkeitspegel errichtet. Die Abstände aufeinanderfolgender, normalerweise 8 bis 9 km voneinander entfernter Pegel wurden mittels Tellurometer, die Polygonwinkel mit einem Präzisionstheodolit gemessen. Für diese Beobachtungsmethode waren sechs Mann, verteilt auf drei Gruppen zu je zwei Mann, nötig.

Das Hauptkapitel behandelt die Verarbeitung der Messdaten und die Berechnung der Eisbewegung. Da sich das Eis ständig bewegt, ändert sich die geometrische Konfiguration des Polygonzuges während des Beobachtungszeitraumes. Zwei Methoden zur Reduktion auf einen bestimmten Zeitpunkt werden ausführlich beschrieben: (1) Zeitreduktion von Beobachtungen. (2) Zeitreduktion von Punktlagen. Zwischen den beiden Messkampagnen kann nur eine lineare Eisbewegung angenommen werden. Es ist jedoch möglich, Beschleunigung und Krümmung der Strömungslinien an all den Polygonpunkten zu bestimmen, deren Polygonwinkel sich beträchtlich von 180° unterscheiden.

Das Resultat der Berechnungen ist das Geschwindigkeitsvektorfeld längs des Polygonzugs. Auffällig ist der rapide Geschwindigkeitsanstieg zwischen McMurdo- und Ross Ice Shelf, die gleichförmige und nahezu parallele Bewegung in der Mitte des Eisschelfs (Maximalgeschwindigkeit 935 m pro Jahr), der Geschwindigkeitsabfall im Nord-Süd-Profil und die systematische Zunahme der Divergenz der Strömungslinien gegen die Eisränder. Sorgfältiges Studium des Geschwindigkeitsvektorfeldes zeigt einige Abweichungen von einer völlig gleichförmigen Verteilung längs des Profiles.

Introduction

Since its discovery by Sir James Clark Ross in 1841, the Ross Ice Shelf, Antarctica, has attracted more and more scientific attention. But it was not until the International Geophysical Year (I.G.Y.), 1957–58, that Crary and others (1962) began to undertake various glaciological and seismological traverses across this part of the white continent. A series of field operations was initiated by J. H. Zumberge, who after his deformation studies at "Camp Michigan" (Zumberge and others, 1960) realized with C. W. M. Swithinbank the importance of the so-called Dawson trail* for long-term glaciological investigations. His "Ross Ice Shelf Studies" consisted of the determination of ice deformation, movement and snow accumulation along this route. During the second traverse of the route (Ross Ice Shelf Traverse, RIST) in the Antarctic summer 1959–60, Swithinbank was able to measure the heights of 1 800 bamboo poles, and to set out simple deformation patterns each 20 miles (32 km) (Zumberge, 1964, p. 71). He also made sun observations at points along the trail. A comparison of the geographical coordinates of these points with the corresponding values of Dawson suggested ice velocities (Zumberge, 1964, p. 67) with errors in places twice as big as the ice velocity itself.

Therefore, when Zumberge was planning a repetition of RIST in 1962–63, W. Hofmann proposed improvements, originating from his geodetic field work with Expédition Glaciologique Internationale au Groenland (EGIG) on the Greenland ice sheet in 1959 (Hofmann, 1964). During the Antarctic summer 1962–63, a geodetic traverse was measured by means of modern tellurometers along the Dawson trail (Hofmann, 1963). Particulars of the instruments and their use were published by Hofmann and others (1964). Due to the accumulation of observational errors in a geodetic traverse, the accuracy of traverse points decreases rapidly with increasing distance from the starting point. Therefore, traverse angles and distances have to be determined with high precision. Only then, and by complying with some special conditions for observing in polar regions, can individual traverse points be determined with a precision one to two orders of magnitude higher than by astronomical means. The traverse, therefore, has been called the "Ross Ice Shelf Survey" (RISS).

In the course of this RISS-I expedition, 114 marking poles were set out and surveyed along the Dawson trail, and also along a profile roughly parallel to the 168° W. meridian. They consisted of 12 ft (3.6 m) aluminium tubes which projected about 6 ft (1.8 m) above the snow surface. During the traverse, Heap and Rundle (1964) re-measured the 1 800 bamboo poles that had been set up in 1958, thus giving for the first time a complete accumulation profile across the northern part of the Ross Ice Shelf.

The measurements were repeated during the Antarctic summer 1965–66 under the leadership of E. Dorrer. The purpose was to re-measure the RISS-I markers using the same geodetic methods. The differences in distance and angle between the measurements would then give the displacement, and hence the actual movement for each marker. The following sections deal with RISS-II and the data processing of both sets of measurements.

Geodetic Field Work

Personnel

Each expedition consisted of six men (for RISS-I see Hofmann and others (1964)). The participants of RISS-II were E. Dorrer as geodesist and field leader, K. Nottarp as electronic specialist, O. Reinwarth as glaciologist, N. O'Hara as geologist and navigator, W. Seufert as assistant geodesist and D. Stelling as assistant glaciologist.

* In December 1958, Major M. Dawson had led a U.S. Army tractor train from "Little America V" almost to McMurdo, and had marked the route by 3 m high bamboo stakes about 350 m apart, and by empty fuel-drum cairns every 20 miles (32 km).

Instruments

During both traverses, the same surveying methods were used. Experience in Greenland (Hofmann, 1964) showed that a geodetic traverse was most accurate if its distances were measured with tellurometers and its angles with a precision theodolite. Unlike the 1959 journey in Greenland, the aerial system was separated from the tellurometer and mounted on a light aluminium tube approximately 4 m high (Nottarp, 1963). It was therefore possible to measure distances of 8 to 11 km directly, almost independently of local topographic features on the ice shelf. Using experience from RISS-I, special extension legs for the theodolite tripod were constructed by Nottarp, thus enabling the observer to sight his angle targets during RISS-II from a standpoint up to 0.5 m higher. The targets were identical with the tellurometer reflectors (diameter 65 cm). Because of the high mounting of the theodolite, traverse angles could be measured even under abnormal atmospheric conditions. One tellurometer (MA I-417) was borrowed from the Ohio State University and two others (MR II-3MV, MRA II-4MV) from the U.S. Army Corps of Engineers at Fort Belvoir, Maryland. A Kern DKM3 precision theodolite had been made available to the party by the Institut für Photogrammetrie und Kartographie at the Technische Hochschule München, Germany, a Zeiss Th 40 theodolite by the Geodätisches Institut of the Technische Hochschule Braunschweig, Germany, and a Kern DKM2 theodolite with astronomical accessories by United States Antarctic Research Programs (USARP).

Equipment

The group was provided with four used Polaris "Sno Traveler" motor toboggans by USARP. One of these motor toboggans broke down at R18 and could not be repaired within reasonable time; it was left behind. Scientific instruments, tents, food, fuel, aluminium tubes, bamboo poles and personal gear were distributed on eleven Nansen sledges, three or four of which had to be dragged behind each motor toboggan.

Method

To eliminate gross errors in the observations and to check the results, distances as well as angles must be measured at least twice and preferably repeatedly. This requires the arrangement of three groups of two men each, distributed over three neighbouring traverse stations (Fig. 1). The measuring process was directed by means of the voice communication channel in the tellurometer system.

The task of the first group after leaving its preceding station was to find the next marker. Along the Dawson trail, between R1 and R30, most of the old bamboo poles could be seen and followed. Later on, a navigation technique similar to that of Black (1962) was used. Sitting or standing and facing backwards on the motor toboggan, the driver sighted back along the track of his sledge train and to a fairly straight line of 12 ft (3.6 m) bamboo poles set

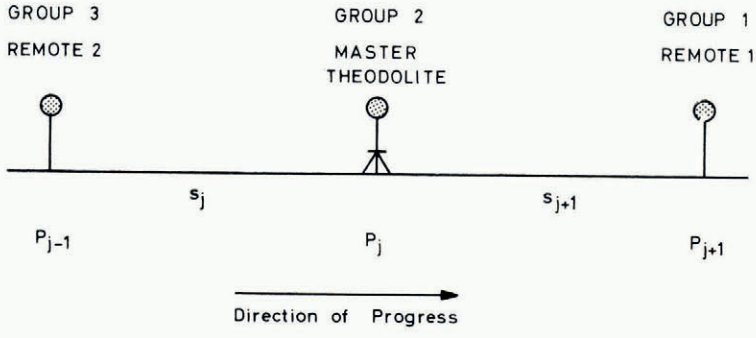

Fig. 1. Arrangement of traverse measurement.

out each kilometre by his companion. After having noted the bearing to the next station by using the RISS-I angle, the navigator never missed the new marker by more than 50 m. Immediately after arrival, the aerial mast was placed vertically on the marker tube and oriented towards the middle group; that is to say, backward by the first group and forward by the third group.

Meanwhile group two (Fig. 1) had set its theodolite vertically above the centre of the upper end of the aluminum tube. This centre was chosen as the reference point to which all measurements were to be related. Normally, the markers of the first traverse could be used directly. Sometimes, however, these old markers were higher than the tripod. In those cases, an auxiliary marker was used a few metres away, the eccentrically measured angles and distances later being reduced to the old marker. Each traverse angle was measured in five full sets as quickly as possible in order to avoid the effects of the tripod sinking into the snow and tripod torsion due to the sun's radiation. In favourable observational conditions, the angle measurement of a single point could be completed in 15 to 20 min.

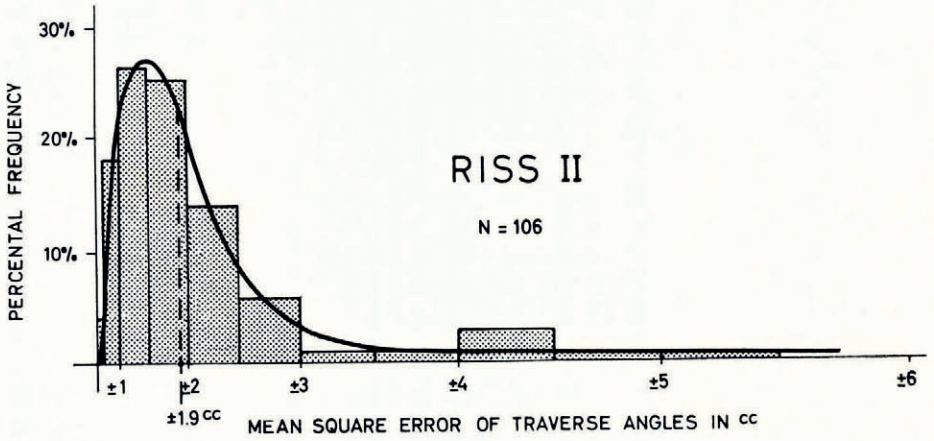

Fig. 2. Frequency distribution of the standard errors of traverse angles.

For the distance measurements, the theodolite and tripod had to be replaced by the tellurometer aerial mast. From each station, group two measured the distance to the forward and to the backward station with its master tellurometer (MA I-417). Ten fine readings were made between the initial and final coarse readings. It was also necessary to make meteorological observations and to measure the inclination of the mast. During the course of the work all traverse distances were measured twice, giving an important check against gross errors. No single distance measurement took more than 15 min.

On each traverse it took about 2 months to measure the 103 traverse stations on the Dawson trail and on the north–south profile (910 km). This gives a rough figure of the rate of measurement using light-weight equipment on a smooth level surface without crevasses such as the northern part of the Ross Ice Shelf.

Accuracy

From a total of 106 angle measurements during the second traverse, a mean square error of $\pm 1.9^{cc}$ (dispersion range 0.3 to 5.2^{cc}) was obtained (Fig. 2). Compared with the corresponding value of the first journey ($\pm 2.3^{cc}$), a remarkable increase in accuracy was noted, due to the experience gained on RISS-I.

Using 101 distances measured back and forth, a mean square error of $\pm 6.7/2 = \pm 3.4$ cm (the same as in RISS-I) resulted for every traverse distance measured twice. As indicated in Figure 3, a systematic error of $4.3/2 = 2.2$ cm with undetermined sign reveals a possible constant deviation between the two remote tellurometers (Fig. 1), probably due to deformation of their antennae. During RISS-I, no similar effect had occurred.

Determination of Surface Movement

Reduction of data

At first, all data observed during both field journeys had to be reduced with respect to deviations from the geometrical model adopted. The transmission time of the electromagnetic waves between two stations depends on the refractive index of air; changes in the pattern frequency of the tellurometer influence the scale of distance measurement. Therefore,

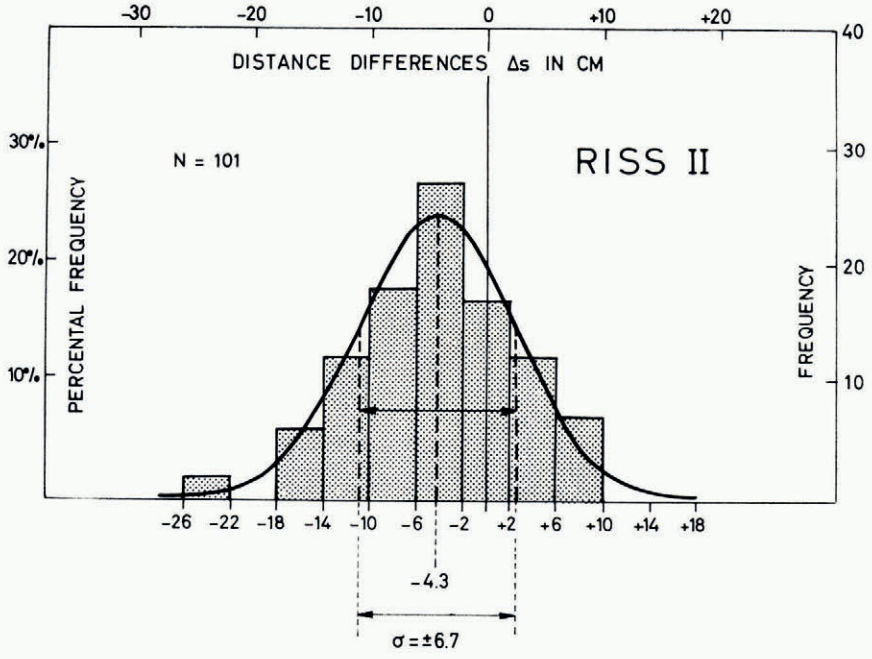

Fig. 3. Frequency distribution of the distance differences between forward and backward measurements.

meteorological reductions due to air pressure, humidity and temperature (Hofmann and others, 1964), and frequency corrections are necessary. Due to the fact that the tellurometer antennae were not exactly vertical, all traverse distances and angles had to be reduced to the reference point defined above.

For each traverse distance measured twice, the arithmetic mean value was calculated. Since both observations were carried out at different instants, this is only correct to a degree depending on the amount of ice deformation. Theoretically, the mean of both distances and the mean of both corresponding observation instants are incoherent quantities.

All angles and distances observed eccentrically on auxiliary markers had to be reduced to the corresponding central marker. Since geographical coordinates refer to an earth ellipsoid coinciding approximately with sea-level, all traverse distances on the ice-shelf surface had to be reduced to sea-level. The corresponding altitudes were taken from Crary and others (1962) and the altitude of Observation Hill is based on the H.O. Chart No. 6712.

Methods

Normally, geodetic measurements are carried out on the rigid earth surface, whose points have fixed relative and absolute positions. However, for measurements over a glacier, the displacement of the surveying point due to the deformation of the surface during the measurement has to be considered. This means that any geometrical observation (angle, azimuth or distance) is valid only for a certain instant (Dorrer, 1967). Measurements combined in the same survey have to be reduced to the same reference time. Deformations and movements in the survey area can be detected and determined by repeated measurements at different times.

The "reduction to epoch" problem has been treated by Swithinbank (1958). Hofmann (1964) has also discussed the reduction of all observations in a glacial survey to a reference time. As small parts of a glacier do not generally change their form very much within short periods, this problem was neglected by Dittrich and Schwarz (1966) for the 100 km long trigonometric chain near the Soviet station Mirny in Antarctica. The geodetic traverse over

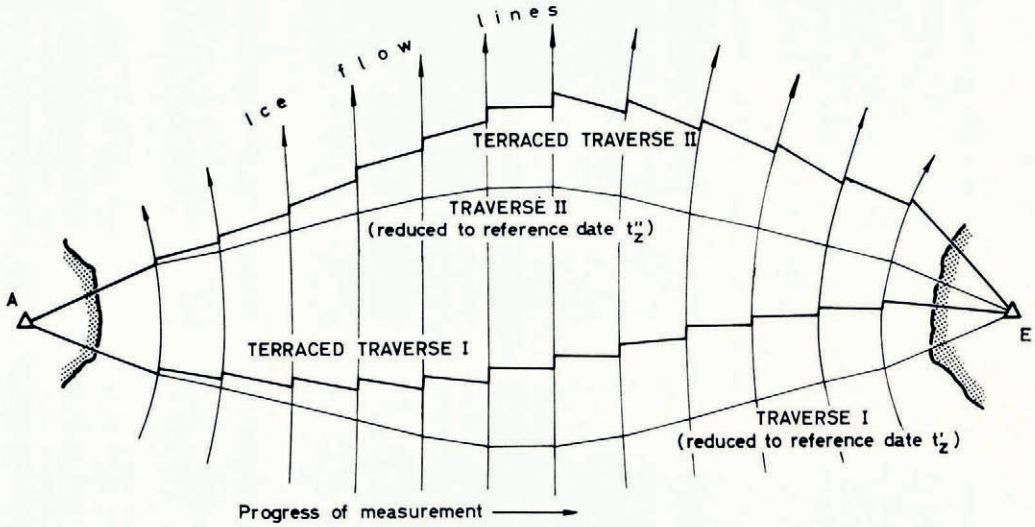

Fig. 4. Terraced traverses caused by time dependency of measurements.

the Ross Ice Shelf, however, extends over a distance of more than 900 km and is tied to a fixed point on rock only at its beginning (it is a so-called "end-free traverse"). Owing to the cumulative propagation of errors of traverse angles, time reduction in this case is essential.

If only two measurements are available, the reduction must be based on the assumption that the movement of the markers took place along straight lines and with constant speed. Neither the curvature of the flow lines nor an acceleration of the trajectory can be derived from such a solution. At the ice margin, however, flow lines curve as the ice conforms to the outline of the land. The start of the RISS traverse (cf. Fig. 11) lies on the McMurdo Ice Shelf in a zone subject to rapid local deformation. Neglecting this would affect at least the directions of the traverse. It is therefore worth considering whether other glaciological surveys in the area might throw light on this problem.

Assuming the traverse points to be moving along straight lines and at constant speed, the time reduction can be made in two distinct ways:

(1) The field observations of the two journeys can be reduced to two reference dates in order to determine the displacements in the period between them. The displacement of all points during the period is computed by comparison between the two series of time-reduced observations. The traverses I and II, reduced to their reference dates t'_z and t''_z, are represented in Figure 4 by thin lines.

(2) The original observations can be used if applied to points whose positions correspond to the actual dates of measurement. These positions are obtained by time reduction along the observed displacement vector. In this case the displacement of all points results from the comparison of two terraced traverses (Fig. 4).

Both methods, if correctly applied, lead to the same final displacement vectors for a certain period, normally one year. As they have both been used on the RISS traverse, they will be described in detail.

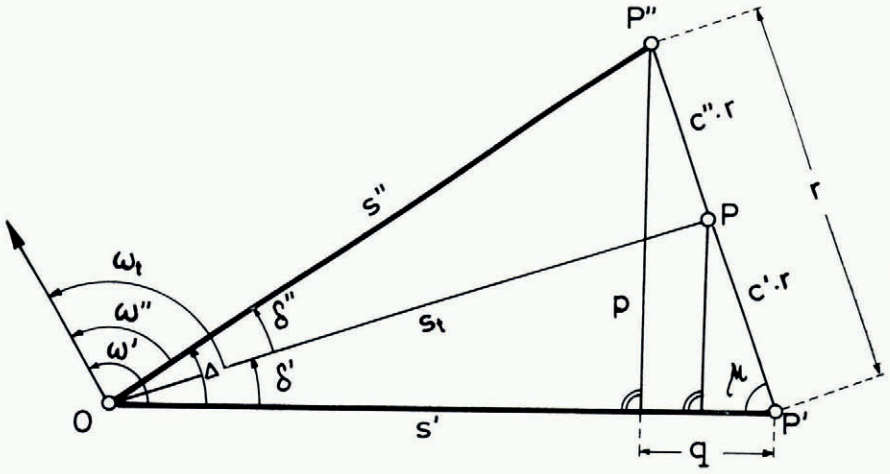

Fig. 5. Time-reduction of observations.

Time reduction of observations (W.H. and W.S.)

The fundamental equations can be derived from Figure 5 in which O is a fixed point whereas P moves along the straight line P′P″ with constant velocity. The traverse angles ω', ω'' and distances s', s'' were measured at times t', t'', respectively. The displacement vector for the time interval $(t''-t')$ is r. The displacement vectors r'_t or r''_t for any time intervals $(t-t')$ or $(t''-t)$ are determined by linear interpolation:

$$r'_t = \left(\frac{t-t'}{t''-t'}\right) r = c'r, \tag{1a}$$

$$r''_t = \left(\frac{t''-t}{t''-t'}\right) r = c''r. \tag{1b}$$

With the denominations in Figure 5 the corresponding values ω_t and s_t can be determined with the following formulae:

$$\begin{aligned} \omega'-\omega'' &= \Delta, \\ p &= r \sin \mu = s'' \sin \Delta, \\ q &= r \cos \mu = s'-s'' \cos \Delta, \end{aligned} \tag{2}$$

$$\tan \delta' = \frac{c'p}{s'-c'q} = \frac{c's'' \sin \Delta}{s'-c'(s'-s'' \cos \Delta)}, \tag{3a}$$

$$s_t = \frac{s'-c'q}{\cos \delta'} = \frac{s'-c'(s'-s'' \cos \Delta)}{\cos \delta'}, \tag{3b}$$

or by exchanging s' with s'' and c' with c''

$$\tan \delta'' = \frac{c''s' \sin \Delta}{s''-c''(s''-s' \cos \Delta)}, \tag{4a}$$

$$s_t = \frac{s''-c''(s''-s' \cos \Delta)}{\cos \delta''}, \tag{4b}$$

$$\omega_t = \omega' - \delta' = \omega'' + \delta''. \tag{5}$$

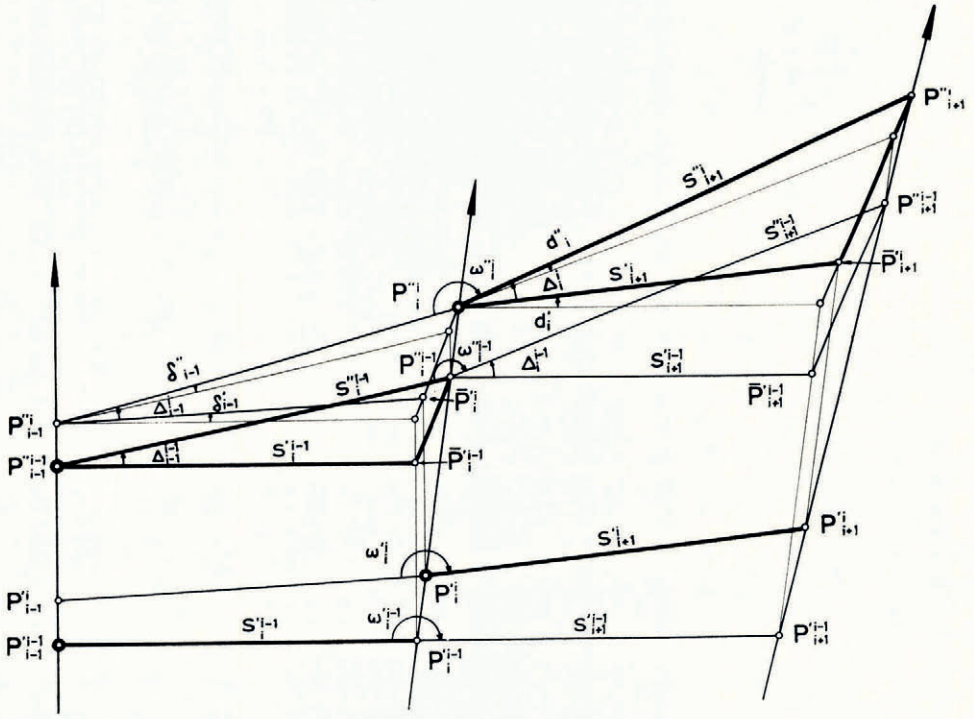

Fig. 6. Time-reduction of observations.

Formulae (3)–(5) show that the time reduction of the observations ω and s depends only on the observations themselves and their changes with time; it can be done without knowledge of the displacement vector r.

In order to reduce errors caused by deviations from the assumed linear movement of P, formulae (3a) and (3b) will be used if $(t-t')$ is small, i.e. for the first traverse, whereas for the same reason formulae (4a) and (4b) are suitable for the second traverse where $(t''-t)$ is small.

For the application of formulae (3)–(5) along the whole traverse, Figure 5 has to be adjusted to the general case where not only P but also O is movable.

Figure 6 shows the straight flow lines of three adjacent points P_{i-1}, P_i, P_{i+1} of the traverse. The positions P′ refer to the first traverse, P″ to the second. The positions P'^{i-1} and P''^{i-1} represent the case that all measurements were executed at the same moments t'_{i-1} and t''_{i-1} on the two traverses.

By parallel shift of the distance s'^{i-1}_i into the position $P''^{i-1}_{i-1}\,\overline{P}'^{i-1}_i$ we originate the triangle $P''^{i-1}_{i-1}\,\overline{P}'^{i-1}_i\,P''^{i-1}_i$. $\overline{P}'^{i-1}_i\,P''^{i-1}_i$ is the vector of the relative displacement between P_{i-1} and P_i in the time interval $(t''_{i-1}-t'_{i-1})$. As all movements are taken to be straight and proportional to time, the length of this vector is proportional to the absolute displacement $P'^{i-1}_i\,P''^{i-1}_i$. Therefore, triangle $P''^{i-1}_{i-1}\,\overline{P}'^{i-1}_i\,P''^{i-1}_i$ corresponds to the reduction triangle $OP'P''$ in Figure 5, and the time reductions of the traverse elements ω and s can be derived in this triangle. The angle Δ^{i-1}_{i-1} is the sum of the differences $\omega'-\omega''$ of the traverse angles from ω_0 to ω_{i-1} between the two traverses; for the present, it may be taken as known.

If the measurements in P'_i and P''_i took place later at t'_i and t''_i, the markers will have moved to the positions P'^i and P''^i. The corresponding reduction triangles are $P''^i_{i-1}\,\overline{P}'^i_i\,P''^i_i$ and $P''^i_i\,\overline{P}'^i_{i+1}\,P''^i_{i+1}$. The triangle $P''^i_i\,\overline{P}'^i_{i+1}\,P''^i_{i+1}$ permits the time reduction of the measurements in P'^i_i and P''^i_i to the times t'_{i-1} and t''_{i-1} in the following way.

The angle Δ^i_i differs from $\Delta_{i-1}{}^i$ by the difference of the measured traverse angles ω'_i and ω''^i_i:

$$\Delta^i_i = \Delta_{i-1}{}^i + \Delta\omega^i_i \qquad (6)$$
$$\Delta\omega^i_i = \omega'^i_i - \omega''^i_i.$$

As Figure 6 shows, angle $\Delta_{i-1}{}^i$ is connected with angle Δ^{i-1}_{i-1} by the equation:

$$\Delta_{i-1}{}^i = \Delta^{i-1}_{i-1} + \delta''_{i-1} - \delta'_{i-1}. \qquad (7)$$

The generally small angles δ'_{i-1} and δ''_{i-1} transform the reduction triangle $P''^{i-1}_{i-1}\,\overline{P}'^{i-1}_i\,P''^{i-1}_i$ into the triangle $P''^i_{i-1}\,\overline{P}'^i_i\,P''^i_i$ and can be computed in the triangle $P''^{i-1}_{i-1}\,\overline{P}'^{i-1}_i\,P''^{i-1}_i$ by application of Equations (3a) and (4a), using the known time intervals $(t'_i-t'_{i-1})$, $(t''_i-t''_{i-1})$ and $(t''_{i-1}-t'_{i-1})$ between the measurements in P_{i-1} and P_i. Combining Equation (7) with (6) gives

$$\Delta^i_i = \Delta^{i-1}_{i-1} + \Delta\omega^i_i + \delta''_{i-1} - \delta'_{i-1}. \qquad (8)$$

With Δ^i_i, all necessary elements of the reduction triangle $P''^i_i\,\overline{P}'^i_{i+1}\,P''^i_{i+1}$ are known.

The time reduction of triangle $P''^i_i\,\overline{P}'^i_{i+1}\,P''^i_{i+1}$ to triangle $P''^{i-1}_i\,\overline{P}'^{i-1}_{i+1}\,P''^{i-1}_{i+1}$ according to formulae (3) and (4) gives the reduced distances s'^{i-1}_{i+1} and s''^{i-1}_{i+1} and the generally small angles d'_i and d''_i.

Finally, as Figure 6 shows, the reduced traverse angles ω'^{i-1}_i and ω''^{i-1}_i can be computed with the formulae:

$$\omega'^{i-1}_i = \omega'^i_i + d'_i - \delta'_{i-1}, \qquad (8a)$$
$$\omega''^{i-1}_i = \omega''^i_i + d''_i - \delta''_{i-1}. \qquad (8b)$$

In this way the traverse elements—angles ω and distances s—of the leg $P_i\,P_{i+1}$, measured at time t_i, can be reduced to any time t_0 if the corresponding elements of the preceding leg $P_{i-1}\,P_i$ are known for the time t_{i-1}. As the elements of the first triangle $P_0\,P'_1\,P''_1$ between the starting point P_0 (Observation Hill) and the first marker P_1 are known as measurements in P_0 at times t'_0 and t''_0, all following measurements can be reduced to the dates t'_0 and t''_0. For that purpose, the angles d'_i and d''_i and the reduced distances s'^0_{i+1} and s''^0_{i+1} have to be computed with the time intervals $(t'_i-t'_0)$ and $t''_i-t''_0)$.

The displacement vectors follow from a comparison of the marker coordinates in both traverses.

Time reduction of positions (E.D.)

The use of original observations requires that they are applied at the points where they were actually measured. The position of points on a surface can be described by differential geometry. The mathematical relations are simple if a reference plane is used. If, however, we consider that all movements take place on the earth ellipsoid (ellipsoid of revolution), the reduction becomes rather complicated. Any points (markers) P on the surface of this ellipsoid

can be indicated by their geographical coordinates $\mathbf{p} = (\lambda, \phi)$, where λ = longitude (positive eastward, negative westward), and ϕ = latitude (positive in the Northern Hemisphere, negative in the Southern Hemisphere).*

If at instants t', t'' a marker P is located at the corresponding positions $\mathbf{p}' = \mathbf{p}(t')$, $\mathbf{p}'' = \mathbf{p}(t'')$, the position of the ice flow line is determined but not its shape. On this line the position of the marker itself is fixed at an arbitrary instant t if the velocity vector $\mathbf{v}$ is known.

The location of a marker P as a function of time can be expanded into a Taylor series in powers of $(t-t_0)$:

$$\mathbf{p}(t) = \mathbf{p}(t_0) + \dot{\mathbf{p}}_0(t-t_0) + \tfrac{1}{2}\ddot{\mathbf{p}}_0(t-t_0)^2 + \dots, \tag{9}$$

where $\dot{\mathbf{p}}_0$ and $\ddot{\mathbf{p}}_0$ are the velocity and acceleration vectors respectively at a reference time t_0. Applying t' and t'' to Equation (9), subtracting the resulting equations from each other, and putting $t_0 = (t'+t'')/2$ gives

$$\mathbf{p}''-\mathbf{p}' = \dot{\mathbf{p}}_0(t''-t') + \mathbf{o}^3. \tag{10}$$

Neglecting all residual terms of higher than second order leads to an average velocity vector

$$\mathbf{v}_0 = \dot{\mathbf{p}}_0 = \frac{\mathbf{p}''-\mathbf{p}'}{t''-t'} = \frac{\Delta\mathbf{p}}{\Delta t}. \tag{11}$$

Since no acceleration vector can be deduced from Equation (10), and therefore no force system assumed to act upon the marker, the flow line has to coincide with the geodesic between P′ and P″. Denoting the metric tensor of the surface by $\mathbf{G}$, and the magnitude of the velocity by v, then

$$v = \frac{r}{t''-t'},$$

where

$$r = \int_{t'}^{t''} (\dot{\mathbf{p}}^T . \mathbf{G} . \dot{\mathbf{p}})^{\frac{1}{2}}\, dt \tag{12}$$

represents the geodetic distance between the two points P′, P″. The variable surface vector $\mathbf{p}$ has to meet the differential equations of the geodesic. This means that Equation (12) is a differential equation which may be solved by any numerical method (see for example Dorrer (1966)).

The reduction procedure will be described by means of Figure 7, which shows the beginning of a terraced traverse repeated after a certain time interval. Starting from a fixed point P_0 and a fixed azimuth from P_0 to a second fixed point P_{-1}, the positions of the first marker P_1 can be computed at instants t'_0, t''_0 at which the angles ω'_0, ω''_0 and distances s'_1, s''_1, respectively, have been measured.

On the earth ellipsoid this computation leads to the solution of two systems of differential equations of the geodesics between P_0 and $P_1'^0 = \mathbf{p}_1(t'_0)$, $P_1''^0 = \mathbf{p}_1(t''_0)$, respectively. This is known in geodetic literature as the "problem of transferring geographical coordinates over long distances" (in the following denoted by "problem I"), for the numerical treatment of which any appropriate method may be used (see for example Dorrer (1964)).† The displacement vector $\mathbf{r}_1$ is now fixed between $P_1'^0$ and $P_1''^0$,‡ and can be determined from Equation (12) which represents the reversal of problem I, viz. the problem of determining distance and azimuth of a geodesic between two known points (problem II §).

* $\mathbf{p}$ is a surface vector and stands for (λ, ϕ).

† In the German language: "Erste geodätische Hauptaufgabe".

‡ The following explanations deal with subscripted variables. Their lower index always denotes the marker's number in the traverse, the upper one distinguishes between several instants of observation.

§ In the German language: "Zweite geodätische Hauptaufgabe".

Since measurements of the angles ω_1', ω_1'' in P_1 and distances s_2', s_2'' have been carried out at different instants t_1', t_1'', respectively, the corresponding positions $\mathbf{p}_1'^1$, $\mathbf{p}_1''^1$ have to be determined on the geodesic through $P_1'^0$ and $P_1''^0$. The small displacements from $P_1'^0$, $P_1''^0$ to $P_1'^1$, $P_1''^1$, denoted by $\delta_0^1 r_1'$, $\delta_0^1 r_1''$, respectively, are defined by

$$\frac{\delta_0^1 r_1'}{t_1'-t_0'} = \frac{\delta_0^1 r_1''}{t_1''-t_0''} = \frac{r_1}{t_0''-t_0'}. \tag{13}$$

$P_1'^1$, $P_1''^1$ can therefore be found by using problem I. To transfer the azimuths between P_0 and $P_1'^1$, $P_1''^1$ to the azimuths between $P_1'^1$, $P_1''^1$ and $P_2'^1$, $P_2''^1$, respectively, at first problem II has to be applied to the geodesics between P_0 and $P_1'^1$, $P_1''^1$ respectively.

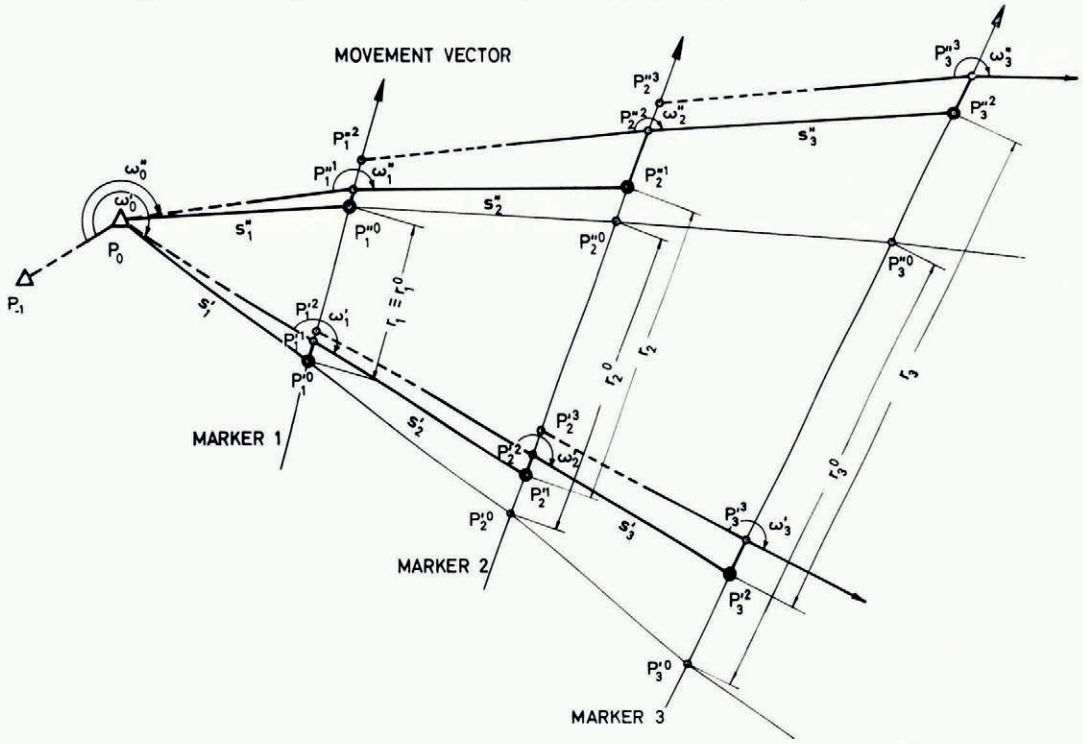

Fig. 7. Geometrical relations at the beginning of a repeated traverse on moving ground (simplified).

The two resulting azimuths $\alpha_{1,0}'^1$, $\alpha_{1,0}''^1$ simply lead to the transferred ones:

$$\alpha_{1,2}'^1 = \alpha_{1,0}'^1 + \omega_1', \tag{14a}$$

$$\alpha_{1,2}''^1 = \alpha_{1,0}''^1 + \omega_1''. \tag{14b}$$

By means of these azimuths and the distances s_2', s_2'', the positions $\mathbf{p}_2'^1 = \mathbf{p}_2(t_1')$ and $\mathbf{p}_2''^1 = \mathbf{p}_2(t_1'')$ of marker P_2 can be determined by problem I, and the procedure described above has to be repeated. From marker P_2 on, however, the transfer of azimuths is possible only if the corresponding positions $\mathbf{p}_1'^2 = \mathbf{p}_1(t_2')$, $\mathbf{p}_1''^2 = \mathbf{p}_1(t_2'')$ of marker P_1 were computed as analogues to $\mathbf{p}_1'^1$, $\mathbf{p}_1''^1$, respectively. The corresponding displacements $\delta_0^{2\prime} r_1 = \|\mathbf{p}_1'^2 - \mathbf{p}_1'^0\|$, $\delta_0^{2\prime\prime} r_1 = \|\mathbf{p}_1''^2 - \mathbf{p}_1''^0\|$* can be determined by using Equation (14):

* $x = \|\mathbf{x}\| = \int_{t_0}^{t} (\dot{\mathbf{x}}^T . \mathbf{G} . \dot{\mathbf{x}})^{1/2}\, dt$ may be denoted as the geodetic norm of a vector $\mathbf{x}$.

$$\frac{\delta_0^{2\prime} r_1}{t_2'-t_0'} = \frac{\delta_0^{2\prime\prime} r_1}{t_2''-t_0''} = \frac{r_1}{t_0''-t_0'} \tag{15}$$

and problem I.

If required, the positions of all markers at their different observation times (two terraced traverses in Figure 4) can now be reduced to a certain reference date which may be chosen arbitrarily unless there are important reasons for a particular time. For the RISS traverse, this applies in the McMurdo Ice Shelf region where great changes of ice velocity occur. Therefore the reference date should be chosen within the period of observations in this region. If this is done, deviations of the supposed straight flow lines from the actual ones will have least effect on the whole traverse. For the sake of simplicity, the dates $t_z' = t_0'$ and $t_z'' = t_0''$ of observations on Observation Hill (P_0) have been taken as reference dates for both traverses. Reducing the markers to these dates analogue to Equations (13) or (15) leads to the positions

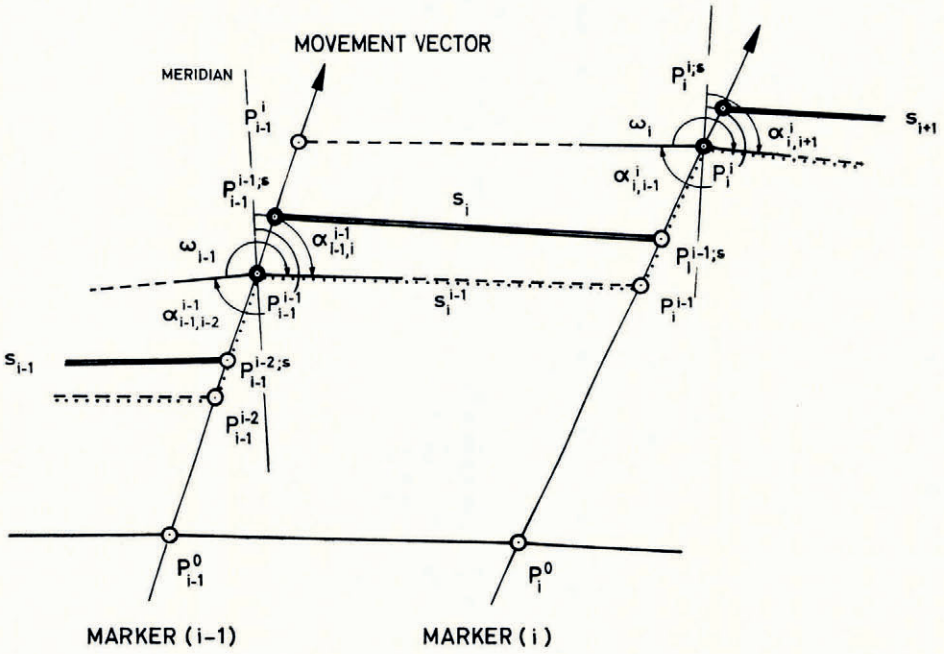

Fig. 8. Measurement conditions between neighbouring stations of a traverse on moving ground.

$\mathbf{p}_i'^0 = \mathbf{p}_i(t_z')$, $\mathbf{p}_i''^0 = \mathbf{p}_i(t_z'')$, $i = 1, 2, \ldots, n$ (Fig. 7) of the two reduced traverses in Figure 4. The geographical coordinates of all traverse markers, listed in the Appendix, are identical with these reduced positions.

The process of computation from a marker P_{i-1} to the next marker P_i requires the solution of problem I six times, and of problem II three times, and, if reduced traverses are wanted, an additional two solutions of problem I.

As the velocity vectors still refer to sea-level, they have to be transferred in reverse to the ice-shelf surface.

Improvement of the method. The method described above can be refined with respect to time reduction and with respect to the acceleration and curvature of the ice movement.

Since at a marker P_{i-1} the traverse angle ω_{i-1} and the traverse distance s_i towards the next marker P_i, $i = 1, 2, \ldots, n$ were normally measured at slightly different times, the two

markers changed their positions relative to each other during the time interval. The computation of P_i by azimuth and distance (problem I) is therefore theoretically incorrect unless s_i is reduced to the date of angle measurement. Figure 8 illustrates the geometrical conditions of the traverse between neighbouring stations.

At a certain time t_{i-1}, the angle ω_{i-1} was measured in $P_{i-1}^{i-1} = \mathbf{p}_{i-1}(t_{i-1})$. The azimuth $\alpha_{i-1,i}^{i-1}$ towards $P_i^{i-1} = \mathbf{p}_i(t_{i-1})$ can then be fixed provided the position of the preceding marker $P_{i-2}^{i-1} = \mathbf{p}_{i-2}(t_{i-1})$ is known at the same time (connection azimuth $\alpha_{i-1,i-2}^{i-1}$). Hence, P_i must lie on the geodetic line that goes through P_{i-1}^{i-1} with an azimuth $\alpha_{i-1,i}^{i-1}$. At another instant $t_{i-1;s}$, distance $s_i = \|\mathbf{p}_i^{i-1;s} - \mathbf{p}_{i-1}^{i-1;s}\|$ was measured between $P_{i-1}^{i-1;s} = \mathbf{p}_{i-1}(t_{i-1;s})$ and $P_i^{i-1;s} = \mathbf{p}_i(t_{i-1;s})$. Since the movement vectors of P_{i-1} and P_i are not parallel, and since $t_{i-1;s} \neq t_{i-1}$, the distances s_i and $s_i^{i-1} = \|\mathbf{p}_i^{i-1} - \mathbf{p}_{i-1}^{i-1}\|$ are not equal. The new position of the marker P_i^{i-1} could be determined exactly by transferring the geographical coordinates $\mathbf{p}_{i-1}^{i-1}$ into $\mathbf{p}_i^{i-1}$ over the distance s_i^{i-1} (problem I), if s_i^{i-1} were known. This distance, however, can only be obtained with mathematical rigour from the solution of an algebraic equation of fourth degree, which numerically is inconvenient. Although $s_i'^{i-1}$ and $s_i''^{i-1}$ could be determined in the case of RISS with sufficient accuracy by assuming a linear dependence of the distance with respect to time, a more general method* may be considered.

Figure 9 illustrates how $s_i'^{i-1}$ and $s_i''^{i-1}$ can be obtained by means of successive approximations, provided that the time interval $t_{i-1;s} - t_{i-1}$ is much smaller than the time difference between both traverses. Proceeding on the assumption that $\mathbf{p}_{i-1}$ is known as a function of time, the positions $\mathbf{p}'^{i-1}_{i-1}$, $\mathbf{p}''^{i-1}_{i-1}$ and $\mathbf{p}'^{i-1;s}_{i-1}$, $\mathbf{p}''^{i-1;s}_{i-1}$ of the marker are fixed (Equation (15)). By means of the known azimuths $\alpha'^{i-1}_{i-1,i}$, $\alpha''^{i-1}_{i-1,i}$ and distances s_i', s_i'', approximate positions $\bar{\mathbf{p}}'^{i-1}_i$, $\bar{\mathbf{p}}''^{i-1}_i$ for $\mathbf{p}'^{i-1}_i$, $\mathbf{p}''^{i-1}_i$, respectively, can be transferred from $\mathbf{p}'^{i-1}_{i-1}$, $\mathbf{p}''^{i-1}_{i-1}$ (problem I). The greater the difference $s_i - s_i^{i-1}$, the more different are the exact and approximate positions. This leads (problem II) to an approximate displacement vector $\bar{\mathbf{r}}_i = \bar{\mathbf{p}}''^{i-1}_i - \bar{\mathbf{p}}'^{i-1}_i$, and to a velocity vector $\bar{\mathbf{v}}_i$ according to Equation (11). Approximate positions $\bar{\mathbf{p}}'^{i-1;s}_i$, $\bar{\mathbf{p}}''^{i-1;s}_i$ can be determined from Equation (9):

$$\bar{\mathbf{p}}_i^{i-1;s} = \bar{\mathbf{p}}_i^{i-1} + \bar{\mathbf{v}}_i(t_{i;s} - t_i).$$

Now, the geodetic distances $\bar{s}_i' = \|\bar{\mathbf{p}}'^{i-1;s}_i - \mathbf{p}'^{i-1;s}_{i-1}\|$, $\bar{s}_i'' = \|\bar{\mathbf{p}}''^{i-1;s}_i - \mathbf{p}''^{i-1;s}_{i-1}\|$, obtained by problem II, have to be compared with the corresponding measured distances s_i', s_i''. From the differences $\delta s_i' = s_i' - \bar{s}_i'$, $\delta s_i'' = s_i'' - \bar{s}_i''$ thus found, the corresponding differences $\delta s'^{i-1}_i$, $\delta s''^{i-1}_i$ can be found by linear interpolation from

$$\frac{\delta s_i' - \delta s'^{i-1}_i}{t'_{i-1;s} - t'_{i-1}} = \frac{\delta s_i'' - \delta s''^{i-1}_i}{t''_{i-1;s} - t''_{i-1}} = \frac{\delta s_i'' - \delta s_i'}{t''_{i-1;s} - t'_{i-1;s}}.$$

Addition of these differences to the measured distances provides better approximations for s'^{i-1}_i, s''^{i-1}_i. The procedure has to be repeated until the differences $\delta s_i'$ and $\delta s_i''$ are equal to zero. The convergence of the recursive process is evident from Figure 9. At the end, the final marker positions $\mathbf{p}'^{i-1}_i$, $\mathbf{p}''^{i-1}_i$, as well as a definite velocity vector $\mathbf{v}_i$, will be obtained.

The second improvement considers that, if the curvature of the flow lines and the change of velocity are known at least approximately, the accuracy of the results can be greatly increased. Especially at the beginning of the traverse in the McMurdo Ice Shelf area, the flow lines depart considerably from straight lines (see Fig. 11). As such data could be obtained from a plot of velocity vectors on the McMurdo Ice Shelf,† it was worth considering them in the computations. However, reliable values for curvature and acceleration could be determined only for the first three RISS markers (Table I).

* If, for instance, curvature and acceleration of the flow lines are considered.

† This plot is the result of an intensive survey of a 10 km marker grid carried out during several Antarctic summers by New Zealand glaciologists (Heine, 1967).

TABLE I. ADDITIONAL VALUES FOR SOME FLOW LINES

Marker	*Curvature* $10^{-6}\ m^{-1}$	*Tangent acceleration* m $year^{-2}$
R1	115	−0.06
R2	90	−0.77
R3	38	−1.85

Knowledge of the curvature c allows us to replace an assumed straight line by an arc of a circle with radius c^{-1}. The straight flow lines shown in the Figures 7, 8 and 9 can therefore be replaced by curves. It is evident that the mathematical relations become still more complicated, even if we neglect earth curvature and earth rotation (Coriolis force).

From Figure 10 there follows a relationship between the length of the arc r_c and the geodetic length of the chord r_g:

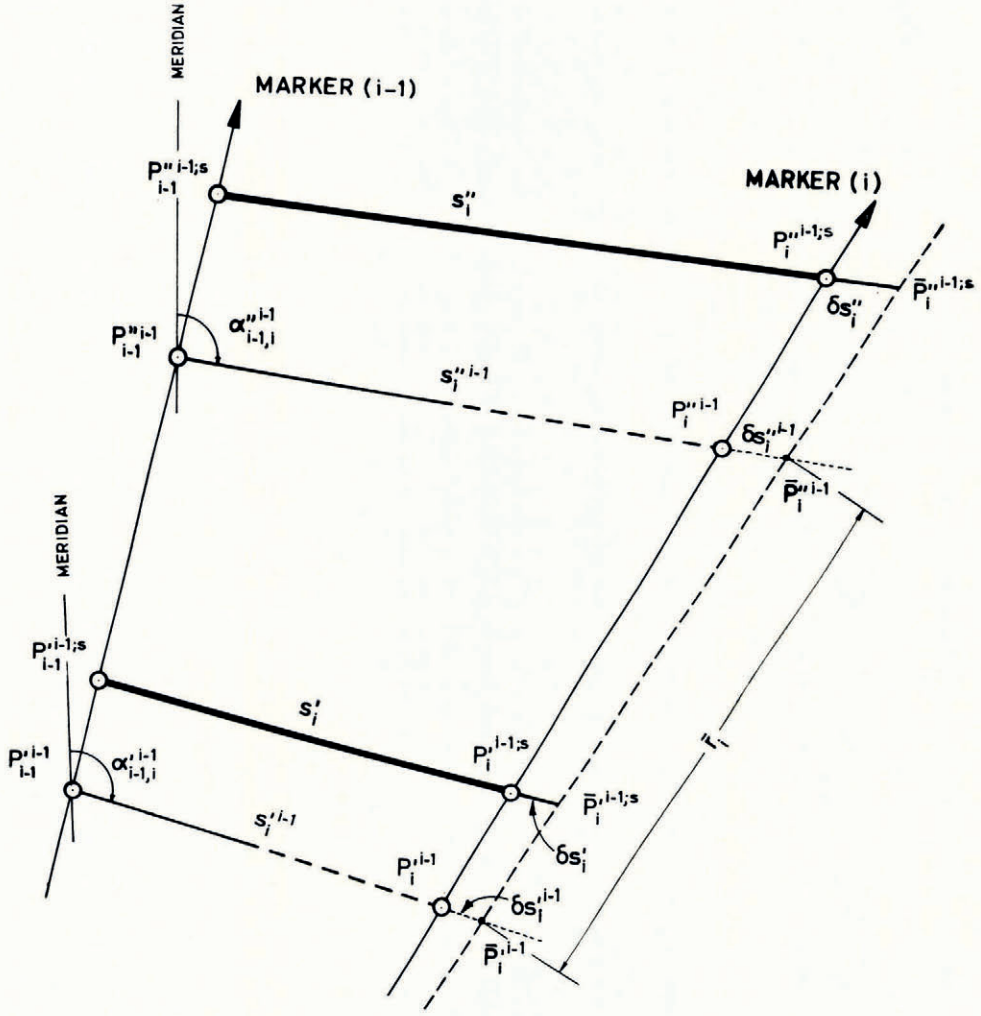

Fig. 9. Iterative solution for the elimination of time differences between consecutive angle and distance measurements.

$$r_c = \frac{\arcsin cr_g/2}{c/2} = r_g + \frac{c^2}{24} r_g^3 + \dots . \tag{16}$$

The whole computation procedure has to be altered with these refinements, i.e. if the positions $\mathbf{p}'^{i-1}_i$, $\mathbf{p}''^{i-1}_i$ of a marker P_i are determined (Figs. 7, 8 and 9), the geodetic length $r_g = \|\mathbf{p}''^{i-1}_i - \mathbf{p}'^{i-1}_i\|$ not only gives the arc length r_c by Equation (16) but also the angle

$$\beta = \frac{\gamma}{2} = \frac{cr_c}{2} \tag{17}$$

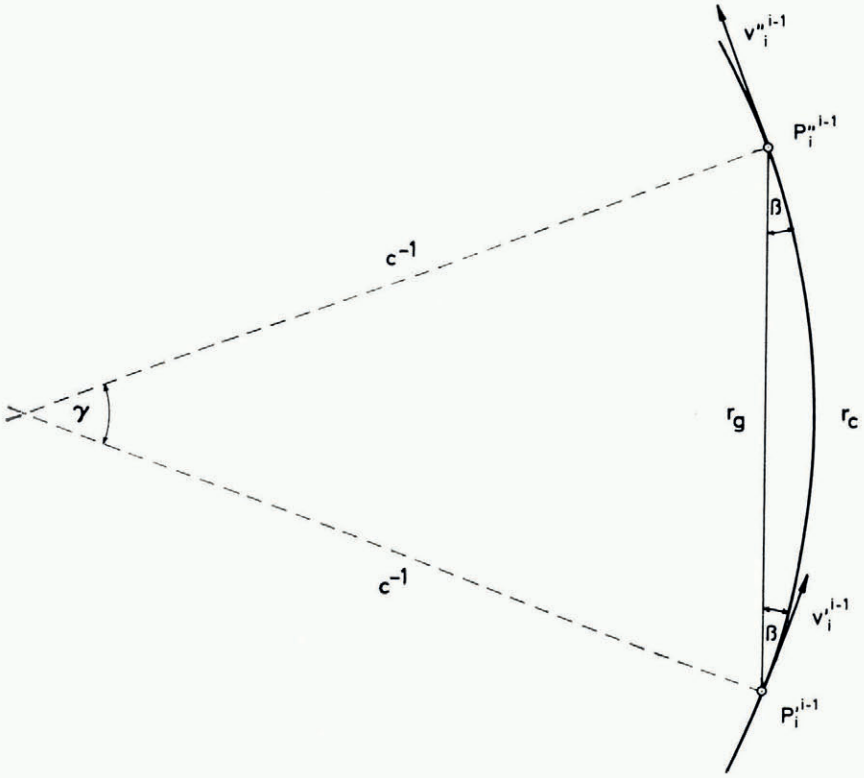

Fig. 10. Flow line with constant curvature.

between chord and arc at the endpoints P'^{i-1}_i, P''^{i-1}_i. The velocity v at these two points results from Equation (9), slightly changed however from its vectorial form into a representation along the flow line. Denoting the arc length by r and the tangent acceleration by a, the differentiation of

$$r(t) = r_0 + v_0(t-t_0) + \tfrac{1}{2}a(t-t_0)^2 + \dots$$

with respect to t then leads to (v_0 from Equation (11))

$$v(t) = v_0 + a(t-t_0) + \dots$$

hence to

$$v'_i = v(t'_{i-1}) = \frac{a}{2}(t''_{i-1} - t'_{i-1}), \tag{18a}$$

$$v''_i = v(t''_{i-1}) = \frac{a}{2}(t''_{i-1} - t'_{i-1}). \tag{18b}$$

Thus the velocity vectors $\mathbf{v}'_i$, $\mathbf{v}''_i$ are determined by Equations (17) and (18), and the positions $\mathbf{p}'^{i-1;s}_i$, $\mathbf{p}''^{i-1;s}_i$, $\mathbf{p}'^{i}_i$, $\mathbf{p}''^{i}_i$ (Fig. 7), or additionally $\mathbf{p}'^{i;s}_i$, $\mathbf{p}''^{i;s}_i$, $\mathbf{p}''^{i+1}_i$, $\mathbf{p}''^{i+1}_i$ (Fig. 8) can be computed by a procedure similar to that described above.

The effect of using these external data becomes evident if we consider the values for c and a of the RISS marker R2 in Table I. By Equations (17) and (18), an angle $\gamma = 2^\circ\,02'$ and a velocity difference $v''-v' = -2.2$ m year^{-1} can be deduced.

Discussion of results

Application of the method described above by means of the reduced field data and Heine's (1967) data (Table I) gives the results listed in the Appendix* and represented graphically in Figure 11.† This figure shows the field of velocity vectors along the RISS traverse. Obvious characteristics are the rapid increase of velocity between McMurdo station and the Ross Ice Shelf, the uniform, nearly parallel movement in the middle of the ice shelf between the markers R33 and R37, and the systematically increasing divergence of the flow lines towards the ice margins.

On the southern leg, a distinct decrease of velocity can be noted as well as a clear change of movement direction due to the turning of the ice flow lines around the western side of Roosevelt Island. The uniform decrease of velocity and the increasing divergence of movement direction along the nearly straight part of the traverse between R57 and R69 makes it possible to extrapolate these values beyond R69 to R76. We find that the region around R77 moves at a velocity of about 300 m year^{-1} almost perpendicular to the ice front west of the Bay of Whales.

Moreover, Figure 11 gives a graphical representation of the strain-rates between each pair of adjacent points on the traverse. These values, which are also listed in the appendix (column 6), give a measure of the relative change of distance per year. Two characteristics are evident. First, a very homogeneous strain field along the Dawson trail with significant variations only at the traverse vertices. Secondly, a high dependence of the strain-rates on the azimuth of the traverse, especially on the southern part of the north–south leg. This is evidently due to the compression caused by a major ice stream coming from Marie Byrd Land and another flowing from the polar plateau through the eastern part of the Queen Maud Range (Giovinetto and others, 1966).

Owing to the zig-zag course of the north–south profile, due to primitive navigation techniques during the first traverse (Hofmann and others, 1964), every station P_i, the traverse angle ω_i of which differs considerably from 180° (Fig. 12), allows us to determine the deformation tensor. For this purpose, the two adjacent strain-rates $\dot{\epsilon}_i$, $\dot{\epsilon}_{i+1}$ and the rate of angle change $\dot{\gamma}_i$ are sufficient, although the accuracy of the eigenvalues and eigenvectors decrease rapidly if ω_i approaches 180°. The maximum and minimum strain-rates, together with their corresponding azimuths, have been computed for many points on the north–south profile but also for a few points on the Dawson trail. It must be noted, however, that these values appear to be significant only for the stations R5, R17, R53, R57 and R69. Though many traverse angles on the north–south profile differ more than 10° from 180°, the errors suggest a greater accuracy than can be expected. The conspicuous major changes of strain-rate (Appendix, column 6) and angle would require much more detailed information about the deformation field than is available from our observations. But this was beyond the scope of RISS.

Although a careful study of the velocity vectors shows some deviations from an entirely uniform distribution along the four straight sections of the traverse between R5 and R69,

* All computations were carried out by a TR 4 computer of the Kommission für Elektronisches Rechnen at the Bayerische Akademie der Wissenschaften, München.

† Traverse points, velocity vectors and strain-rate "rectangles" have been plotted automatically by a ZUSE Z 64 graphomat.

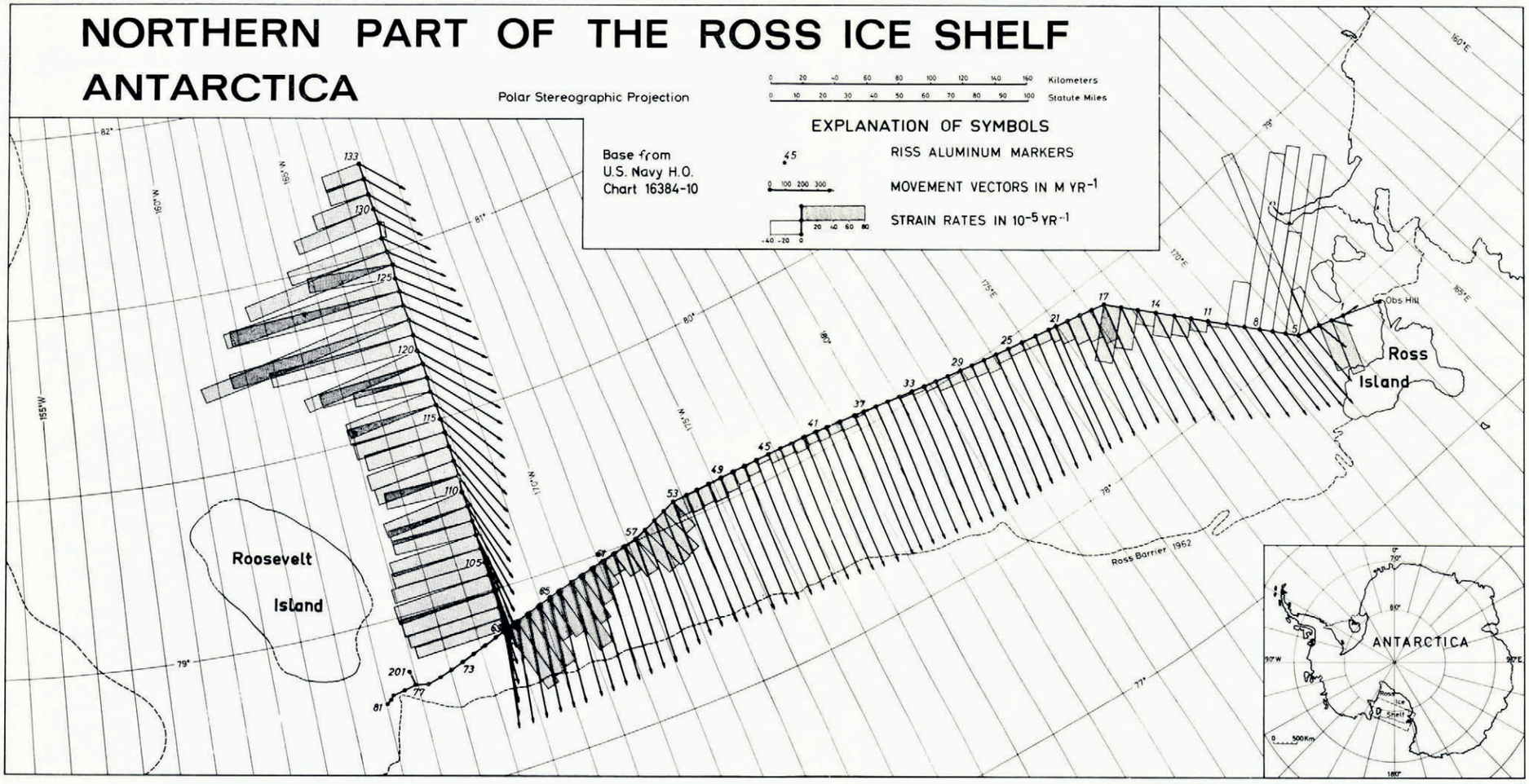

Fig. 11. Map of the northern part of the Ross Ice Shelf, Antarctica, showing the positions of the RISS aluminium markers, the movement vectors (m year^{-1}) and the strain-rates (10^{-5} year^{-1}).

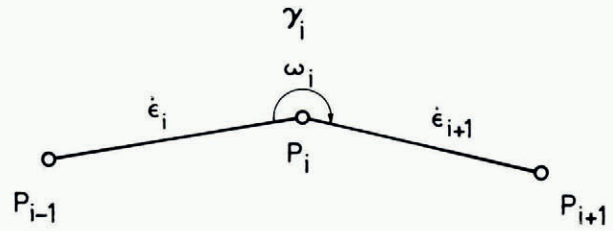

Fig. 12. Adjacent strain-rates and angle change-rate at a traverse point P_i.

velocity changes reveal a more detailed picture. The changes of velocity vectors along all traverse distances (except between R1 and R5), reduced to unit length, are shown in Figure 13. These changes are equivalent to the relative movement vectors between consecutive markers and they depend mainly on the corresponding direction of progress in the velocity vector field. This is evident at the traverse vertices R17, R53, R57, R69 and in the whole north–south profile. For each velocity-change vector the component parallel to its traverse distance is identical to the strain-rate, shown in Figure 11. Notable points lie between R8 and R10, where the border effect of Minna Bluff and Ross Island probably comes to an end, and between R120 and R133.

The velocity-change vectors around the traverse vertices, where the traverse angles differ considerably from 180°, enable us to determine the acceleration and curvature of the ice flow line at these points. The results are shown in Table II. According to this, R5 is slowed down considerably, but R17 still has a negative acceleration.

TABLE II. CURVATURE AND ACCELERATION VALUES FOR THE TRAVERSE VERTICES

Marker	*Curvature* 10^{-6} m^{-1}	*Tangent acceleration* m year^{-2}
R5	27	−9
R17	2.0	−2.9
R69	−5.3	1.2

CONCLUSIONS

In spite of the geodetic character of the field work and data processing in this study, the results obtained are of major glaciological significance. The small expenditure in terms of personnel, equipment and money shows the efficiency of an operation of this kind extending over two Antarctic summer seasons. Use of the same method over inland ice sheets rather than ice shelves would of course need a different type of organization and different vehicles. Although further simplification might be considered (for instance, a reduction of personnel from three groups to two groups of two men each), such changes would be possible only at the expense of accuracy and of reliability of the observations and their results. To achieve a greater accuracy also for points farthest from the fixed starting points, there are two possibilities: (1) Measurement of auxiliary azimuths systematically distributed over the whole traverse, and (2) tying both ends of the traverse to fixed points. The rather sophisticated surveying technique used requires at least one specialist in electronics and one for surveying. In order to encourage further movement studies on the Ross Ice Shelf, all RISS markers were extended to a height above the snow level which ought to keep them visible at least until the 1969–70 summer.

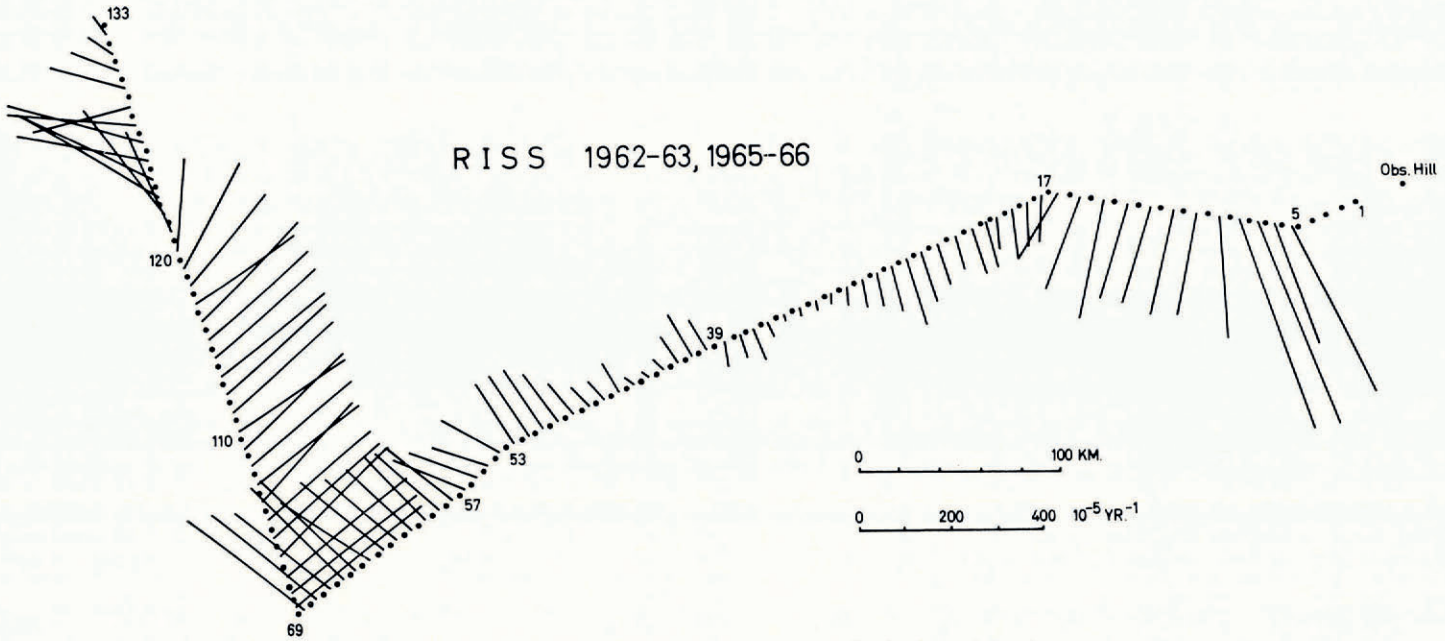

Fig. 13. Velocity vector changes along the traverse and reduced to unit length.

ACKNOWLEDGEMENTS

The field work and data analysis were supported by grants from the National Science Foundation to the University of Michigan and to Grand Valley State College. President J. H. Zumberge was Principal Investigator. Logistic support was provided by Air Development Squadron Six of the U.S. Navy. Help and advice by Professor Dr E. Gotthardt, München, is gratefully acknowledged. Individuals whose help in the field work or in data reduction contributed to this publication are: K. Nottarp, J. A. Heap, A. S. Rundle, W. C. Campbell, O. Reinwarth, N. O'Hara, D. Stelling, A. J. Heine, D. Weber, M. Stephani. The authors wish to express their thanks to C. W. M. Swithinbank for carefully reading and improving this manuscript, and for his suggestions.

MS. received 19 December 1967

REFERENCES

Black, H. P. 1962. A navigation device for steering vehicles in featureless terrain. *Polar Record*, Vol. 11, No. 72 p. 296–98.

Crary, A. P., *and others*. 1962. Glaciological studies of the Ross Ice Shelf, Antarctica, 1957–1960, by A. P. Crary, E. S. Robinson, H. F. Bennett and W. W. Boyd, Jr. *IGY Glaciological Report Series* (New York), No. 6.

Dittrich, G., *and* Schwarz, G. 1966. Die geodätischen Arbeiten der deutschen Gruppe während der 7. sowjetischen Antarktis-Expedition 1962. *Nationalkomitee für Geodäsie und Geophysik der Deutschen Demokratischen Republik bei der Deutschen Akademie der Wissenschaften zu Berlin. Fachgruppe Geodäsie*, Reihe 3, Ht. 5.

Dorrer, E. 1964. Algorithm 240 coordinates on an ellipsoid (Z). *Communications of the Association for Computing Machinery*, Vol. 7, No. 9, p. 546.

Dorrer, E. 1966. Direkte numerische Lösung der geodätischen Hauptaufgaben auf Rotationsflächen. *Deutsche Geodätische Kommission bei der Bayerischen Akademie der Wissenschaften*, Reihe C, Nr. 90.

Dorrer, E. 1967. Die Bestimmung der Oberflächengeschwindigkeit ausgedehnter Gletschergebiete. Ein Beitrag zur Erfassung horizontaler Bodenbewegungen mit geodätischen Methoden. *Zeitschrift für Vermessungswesen*, 1967, p. 183–89.

Giovinetto, M. B., *and others*. 1966. The regime of the western part of the Ross Ice Shelf drainage system, by M. [B.] Giovinetto, E. S. Robinson and C. W. M. Swithinbank. *Journal of Glaciology*, Vol. 6, No. 43, p. 55–68.

Heap, J. A., *and* Rundle, A. S. 1964. Snow accumulation on the Ross Ice Shelf, Antarctica. (*In* Mellor, M., *ed. Antarctic snow and ice studies*. Washington, D.C., American Geophysical Union, p. 119–25. (Antarctic Research Series, Vol. 2.))

Heine, A. J. 1967. The McMurdo Ice Shelf, Antarctica: a preliminary report. *New Zealand Journal of Geology and Geophysics*, Vol. 10, No. 2, p. 474–78.

Hofmann, W. 1963. Geodätisch-glaziologische Arbeiten in der Antarktis. *Zeitschrift für Vermessungswesen*, 1963, p. 255–65.

Hofmann, W. 1964. Die geodätische Lagemessung über das grönländische Inlandeis der Internationalen Glaziologischen Grönland-Expedition (EGIG) 1959. *Meddelelser om Grønland*, Bd. 173, Nr. 6.

Hofmann, W., *and others*. 1964. The Ross Ice Shelf Survey (RISS), 1962–1963, by W. Hofmann, E. Dorrer and K. Nottarp. (*In* Mellor, M., *ed. Antarctic snow and ice studies*. Washington, D.C., American Geophysical Union, p. 83–118. (Antarctic Research Series, Vol. 2.))

Nottarp, K. 1963. Hochantennen für Tellurometermessungen in der Antarktis. *Allgemeine Vermessungsnachrichten*, 1963, Ht. 8, p. 304–07.

Swithinbank, C. W. M. 1958. Glaciology. I. The movement of the ice shelf at Maudheim. *Norwegian–British–Swedish Antarctic Expedition, 1949–52. Scientific Results*, Vol. 3, C.

Zumberge, J. H. 1964. Horizontal strain and absolute movement of the Ross Ice Shelf between Ross Island and Roosevelt Island, Antarctica, 1958–1963. (*In* Mellor, M., *ed. Antarctic snow and ice studies*. Washington, D.C., American Geophysical Union, p. 65–81. (Antarctic Research Series, Vol. 2.))

Zumberge, J. H., *and others*. 1960. Deformation of the Ross Ice Shelf near the Bay of Whales, Antarctica, by J. H. Zumberge, M. [B.] Giovinetto, R. Kehle and J. [R.] Reid. *IGY Glaciological Report Series* (New York), No. 3.

APPENDIX

Station	Longitude	Latitude	Velocity	Azimuth	Strain-rate	Azimuth
	RISS–I: 2.11.1962, 19* RISS–II: 12.11.1965, 16*		m year^{-1}		10^{-5} year^{-1}	
R0	166° 41′ 16.6″ E.	77° 51′ 12.4″ S.				
R1	167 39 50.23 E. 167 38 58.93	77 56 10.16 S. 77 56 08.53	111.1	278° 39′ 36″	+70.9	108° 40′ 39″
R2	167 58 25.23 E. 167 57 50.98	77 57 34.01 S. 77 57 23.41	131.0	326 00 50	+59.5	108 09 02
R3	168 18 18.29 E. 168 18 00.57	77 59 00.79 S. 77 58 40.94	206.8	349 27 30	−53.5	103 33 26
R4	168 35 54.01 E. 168 35 56.32	78 00 04.14 S. 77 59 24.79	403.1	0 41 58	−239.5	105 55 40
R5	168 53 37.67 E. 168 53 48.70	78 01 14.24 S. 78 00 21.61	539.6	2 29 39	−224.6	139 23 19
R6	169 07 15.61 E. 169 07 29.45	78 04 33.84 S. 78 03 38.19	570.7	2 56 39	−129.2	139 15 00
R7	169 21 07.95 E. 169 21 24.45	78 07 54.50 S. 78 06 56.83	591.8	3 22 15	−230.0	138 42 08
R8	169 35 04.16 E. 169 35 25.39	78 11 12.35 S. 78 10 11.20	628.0	4 04 06	−218.8	138 08 47
R9	169 52 00.47 E. 169 52 28.13	78 15 07.13 S. 78 14 01.75	672.2	4 55 42	−54.8	138 27 11
R10	170 11 06.44 E. 170 11 40.57	78 19 31.80 S. 78 18 24.15	696.5	5 50 04	+58.5	138 26 05
R11	170 32 03.71 E. 170 32 45.40	78 24 19.75 S. 78 23 10.47	714.8	6 54 16	+14.3	137 38 45
R12	170 51 11.20 E. 170 52 00.48	78 28 33.87 S. 78 27 23.07	732.2	7 55 27	+23.2	137 37 26
R13	171 10 20.48 E. 171 11 17.11	78 32 46.57 S. 78 31 34.40	748.3	8 51 58	+27.3	137 25 13
R14	171 31 28.32 E. 171 32 32.87	78 37 21.57 S. 78 36 07.96	765.2	9 49 33	+17.2	136 40 25
R15	171 52 43.38 E. 171 53 57.25	78 41 49.65 S. 78 40 34.15	787.5	10 52 06	+49.1	136 41 39
R16	172 12 40.14 E. 172 14 01.99	78 45 59.50 S. 78 44 42.82	802.4	11 45 40	+68.8	136 36 41
R17	172 33 10.53 E. 172 34 39.20	78 50 13.65 S. 78 48 56.29	811.8	12 31 33	+44.9	103 16 07
R18	172 55 40.60 E. 172 57 09.52	78 51 15.69 S. 78 49 57.60	819.1	12 25 41	+35.3	102 37 38
R19	173 18 03.69 E. 173 19 32.35	78 52 14.25 S. 78 50 55.44	826.1	12 16 02	+31.6	102 04 00
R20	173 40 21.69 E. 173 41 50.01	78 53 09.91 S. 78 51 50.27	834.3	12 04 48	+23.6	102 05 16

* Day, month, year and hour to which observations have been reduced.

Station	*Longitude*	*Latitude*	*Velocity*	*Azimuth*	*Strain-rate*	*Azimuth*
			m year^{-1}		10^{-5} year^{-1}	
R21	174° 02′ 00.48″E. 174 03 27.86	78° 54′ 03.84″S. 78 52 43.61	839.8	11° 51′ 20″		
					+17.0	101° 06′ 57″
R22	174 15 33.61 E. 174 17 00.34	78 54 34.87 S. 78 53 14.13	844.7	11 41 15		
					+12.3	101 14 02
R23	174 40 31.10 E. 174 41 56.45	78 55 32.62 S. 78 54 10.86	854.2	11 21 07		
					+11.0	100 51 06
R24	175 06 07.28 E. 175 07 30.79	78 56 29.57 S. 78 55 07.05	861.2	10 59 57		
					+10.2	100 31 04
R25	175 31 52.28 E. 175 33 12.75	78 57 23.75 S. 78 56 01.59	869.6	10 38 19		
					+12.0	99 54 35
R26	175 54 54.89 E. 175 56 15.14	78 58 11.85 S. 78 56 47.43	879.0	10 19 15		
					+18.4	99 27 30
R27	176 17 46.59 E. 176 19 05.80	78 58 56.22 S. 78 57 30.58	891.0	10 02 09		
					+16.2	99 17 52
R28	176 40 30.04 E. 176 41 47.74	78 59 39.34 S. 78 58 12.84	899.1	9 44 37		
					+14.7	99 04 22
R29	177 02 21.34 E. 177 03 37.33	79 00 19.64 S. 78 58 52.52	904.8	9 27 24		
					+13.9	98 35 27
R30	177 26 00.30 E. 177 27 14.26	79 01 00.82 S. 78 59 33.14	909.8	9 08 27		
					+14.4	98 23 29
R31	177 48 49.64 E. 177 50 01.50	79 01 39.51 S. 79 00 11.44	913.0	8 50 23		
					+8.0	98 04 31
R32	178 10 29.28 E. 178 11 38.76	79 02 14.72 S. 79 00 46.44	914.4	8 31 25		
					+5.4	97 29 41
R33	178 34 10.36 E. 178 35 17.12	79 02 50.40 S. 79 01 21.87	916.2	8 09 48		
					+3.2	97 27 40
R34	178 57 29.92 E. 178 58 33.85	79 03 25.32 S. 79 01 56.59	917.5	7 47 53		
					+1.2	96 56 59
R35	179 20 41.78 E. 179 21 42.79	79 03 57.62 S. 79 02 28.71	918.5	7 25 28		
					+0.1	96 30 12
R36	179 43 26.21 E. 179 44 24.37	79 04 27.29 S. 79 02 58.06	921.1	7 03 05		
					+1.6	96 02 28
R37	179 53 41.95 W. 179 52 46.45	79 04 55.14 S. 79 03 25.27	926.9	6 40 49		
					+4.2	95 38 27
R38	179 36 16.21 W. 179 35 22.76	79 05 14.89 S. 79 03 44.67	930.1	6 24 30		
					+13.0	95 23 44
R39	179 07 30.89 W. 179 06 40.38	79 05 46.05 S. 79 04 15.25	935.3	6 00 52		
					+11.8	95 17 58
R40	178 41 53.47 W. 178 41 06.21	79 06 12.70 S. 79 04 42.52	928.3	5 39 56		
					+13.6	94 57 45
R41	178 21 17.57 W. 178 20 32.90	79 06 32.62 S. 79 05 03.13	920.8	5 23 42		
					+11.8	93 03 43
R42	177 57 48.31 W. 177 57 06.44	79 06 46.60 S. 79 05 17.62	915.0	5 05 07		
					+14.5	92 31 55

Station	*Longitude*	*Latitude*	*Velocity*	*Azimuth*	*Strain-rate*	*Azimuth*
			m year^{-1}		10^{-5} year^{-1}	
R43	177° 34′ 40.34″ W.	79° 06′ 58.08″ S.	912.5	4° 47′ 16″		
	177 34 01.01	79 05 29.32			+12.1	92° 11′ 44″
R44	177 11 09.06 W.	79 07 08.24 S.	910.9	4 28 13		
	177 10 32.39	79 05 39.59			+12.3	91 44 43
R45	176 48 12.76 W.	79 07 16.09 S.	909.2	4 09 46		
	176 47 38.67	79 05 47.57			+6.6	91 33 13
R46	176 24 26.02 W.	79 07 23.11 S.	903.1	3 49 32		
	176 23 54.89	79 05 55.14			+14.2	91 03 58
R47	176 01 08.30 W.	79 07 27.82 S.	899.1	3 31 48		
	176 00 39.70	79 06 00.22			+18.0	90 40 24
R48	175 38 48.43 W.	79 07 30.59 S.	894.8	3 16 05		
	175 38 22.07	79 06 03.38			+20.8	90 20 12
R49	175 14 51.93 W.	79 07 31.84 S.	887.9	3 00 40		
	175 14 27.82	79 06 05.28			+24.4	89 30 20
R50	174 51 13.32 W.	79 07 29.01 S.	877.7	2 47 44		
	174 50 51.20	79 06 03.43			+21.9	89 07 03
R51	174 27 56.37 W.	79 07 24.33 S.	865.6	2 34 56		
	174 27 36.22	79 05 59.92			+23.5	88 44 55
R52	174 07 32.44 W.	79 07 18.72 S.	854.6	2 24 32		
	174 07 13.88	79 05 55.37			+21.2	88 24 05
R53	173 41 30.98 W.	79 07 09.78 S.	840.7	2 10 44		
	173 41 14.47	79 05 47.77			+40.2	69 09 21
R54	173 19 40.18 W.	79 05 34.80 S.	831.2	2 20 42		
	173 19 22.65	79 04 13.72			+62.6	68 17 17
R55	172 57 56.07 W.	79 03 55.84 S.	824.1	2 36 12		
	172 57 36.83	79 02 35.48			+64.2	68 01 42
R56	172 36 27.04 W.	79 02 16.43 S.	816.0	2 55 05		
	172 36 05.74	79 00 56.88			+61.3	67 37 54
R57	172 15 08.63 W.	79 00 35.55 S.	806.9	3 16 03		
	172 14 45.10	78 59 16.91			+48.5	76 40 19
R58	171 52 17.26 W.	78 59 32.81 S.	794.5	3 27 41		
	171 51 52.77	78 58 15.40			+37.0	76 16 37
R59	171 29 45.06 W.	78 58 28.95 S.	781.6	3 36 59		
	171 29 19.92	78 57 12.80			+25.1	75 54 28
R60	171 07 38.86 W.	78 57 24.43 S.	768.2	3 43 55		
	171 07 13.41	78 56 09.60			+35.5	75 24 41
R61	170 45 26.36 W.	78 56 17.14 S.	754.9	3 55 55		
	170 45 00.05	78 55 03.62			+47.2	74 57 08
R62	170 23 16.77 W.	78 55 07.65 S.	741.3	4 14 40		
	170 22 48.93	78 53 55.49			+63.2	74 39 21
R63	170 03 00.09 W.	78 54 02.52 S.	726.9	4 42 51		
	170 02 29.83	78 52 51.80			+87.7	74 10 55
R64	169 37 12.91 W.	78 52 36.91 S.	710.3	5 31 08		
	169 36 38.38	78 51 27.89			+57.8	74 00 35

Station	*Longitude*	*Latitude*	*Velocity*	*Azimuth*	*Strain-rate*	*Azimuth*
			m year^{-1}		10^{-5} year^{-1}	
R65	169° 17′ 11.75″ W. 169 16 34.34	78° 51′ 29.35″ S. 78 50 22.10	692.9	6° 08′ 33″		
R66	168 56 12.43 W. 168 55 32.01	78 50 16.46 S. 78 49 11.11	674.2	6 50 08	+52.4	73° 35′ 53″
R67	168 33 31.33 W. 168 32 46.65	78 48 55.42 S. 78 47 51.87	657.1	7 46 18	+79.9	73 09 19
R68	168 11 50.73 W. 168 11 01.39	78 47 36.25 S. 78 46 34.64	638.7	8 51 21	+82.7	72 51 20
R69	167 50 21.43 W. 167 49 26.84	78 46 16.35 S. 78 45 16.77	619.9	10 07 35	+90.6	72 36 33
R101	167 50 18.87 W. 167 49 35.31	78 49 57.63 S. 78 48 58.82	608.6	8 10 11	+115.0	180 10 11
R102	167 50 28.74 W. 167 49 56.78	78 53 50.27 S. 78 52 52.27	597.5	6 03 42	+119.5	180 45 59
R103	167 50 51.05 W. 167 50 35.22	78 59 18.17 S. 78 58 21.34	582.9	3 02 58	+123.3	181 02 18
R104	167 50 06.28 W. 167 50 07.49	79 05 15.36 S. 79 04 19.95	567.6	359 45 45	+125.0	178 54 59
R105	167 50 19.93 W. 167 50 33.96	79 09 53.83 S. 79 08 59.42	558.1	357 13 25	+121.9	180 47 52
R106	167 50 43.88 W. 167 51 11.59	79 14 57.75 S. 79 14 04.35	549.5	354 27 55	+116.0	181 06 20
R107	167 50 10.81 W. 167 50 51.93	79 19 57.44 S. 79 19 05.12	541.6	351 42 51	+113.7	179 05 01
R108	167 51 31.19 W. 167 52 25.71	79 24 55.05 S. 79 24 03.53	537.7	348 59 26	+103.2	183 06 23
R109	167 51 33.47 W. 167 52 42.03	79 29 58.24 S. 79 29 07.66	533.8	346 06 53	+103.2	180 20 28
R110	167 49 27.69 W. 167 50 50.44	79 34 57.47 S. 79 34 08.03	529.2	343 08 56	+105.6	175 54 25
R111	167 51 55.88 W. 167 53 33.26	79 40 05.30 S. 79 39 16.51	530.9	340 17 22	+95.0	185 13 03
R112	167 51 08.68 W. 167 53 00.75	79 45 06.74 S. 79 44 18.97	530.4	337 19 44	+104.6	178 40 10
R113	167 50 27.77 W. 167 52 34.62	79 50 04.62 S. 79 49 17.88	531.0	334 23 22	+108.0	178 52 49
R114	167 51 08.25 W. 167 53 30.13	79 55 01.70 S. 79 54 15.82	534.6	331 33 04	+104.2	181 38 51
R115	167 51 13.20 W. 167 53 49.79	79 59 49.36 S. 79 59 04.45	538.0	328 46 47	+113.5	180 26 57
R116	167 51 41.31 W. 167 54 33.90	80 05 01.72 S. 80 04 17.86	543.0	325 51 39	+116.0	181 09 59
R117	167 49 10.37 W. 167 52 18.86	80 10 04.28 S. 80 09 21.69	547.1	322 54 09	+114.3	175 23 44
					+94.4	185 23 39

Station	*Longitude*	*Latitude*	*Velocity*	*Azimuth*	*Strain-rate*	*Azimuth*
			m year^{-1}		10^{-5} year^{-1}	
R118	167° 51′ 50.11″ W.	80° 15′ 06.56″ S.	556.4	320° 35′ 30″		
	167 55 13.61	80 14 24.60			+134.8	180° 35′ 57″
R119	167 52 01.34 W.	80 20 01.76 S.	559.9	318 15 25		
	167 55 37.90	80 19 20.98			+154.3	173 32 55
R120	167 48 44.62 W.	80 24 42.87 S.	559.6	315 54 40		
	167 52 32.64	80 24 03.64			+184.7	183 05 36
R121	167 50 22.11 W.	80 29 52.00 S.	552.6	314 07 14		
	167 54 16.52	80 29 14.45			+233.5	181 02 29
R122	167 50 55.38 W.	80 34 55.35 S.	535.8	312 36 10		
	167 54 50.48	80 34 19.95			+272.3	175 13 49
R123	167 48 18.23 W.	80 40 04.53 S.	511.7	311 09 15		
	167 52 10.01	80 39 31.66			+217.9	184 07 02
R124	167 50 36.31 W.	80 45 01.71 S.	483.4	310 43 33		
	167 54 18.63	80 44 30.92			+225.4	179 12 51
R125	167 50 17.55 W.	80 49 48.40 S.	454.7	310 31 57		
	167 53 49.10	80 49 19.56			+108.0	187 27 34
R126	167 54 28.87 W.	80 54 44.01 S.	428.4	311 17 34		
	167 57 47.69	80 54 16.41			+191.4	174 57 32
R127	167 51 45.67 W.	80 59 46.58 S.	400.2	311 44 23		
	167 54 51.80	80 59 20.58			+126.3	176 19 34
R128	167 49 48.27 W.	81 04 48.48 S.	375.6	312 56 31		
	167 52 41.26	81 04 23.51			−6.5	187 06 51
R129	167 53 58.32 W.	81 09 49.85 S.	359.4	315 01 25		
	167 56 39.64	81 09 25.04			+106.7	175 28 11
R130	167 51 28.24 W.	81 14 46.37 S.	343.8	315 29 10		
	167 54 02.75	81 14 22.44			+74.3	177 01 34
R131	167 49 47.74 W.	81 19 45.09 S.	333.5	315 39 44		
	167 52 18.59	81 19 21.80			+48.3	180 55 35
R132	167 50 21.30 W.	81 24 51.60 S.	327.7	315 33 40		
	167 52 51.21	81 24 28.77			+49.1	177 59 28
R133	167 49 08.54 W.	81 29 58.17 S.	323.4	315 08 28		
	167 51 39.09	81 29 35.80				